Surface Science 605 (2011) 681–688

Contents lists available at ScienceDirect

Surface Science

journal homepage: www.elsevier.com/ locate/susc

A theoretical study of CO adsorption on FeCo(100) and the effect of alloying

Panithita Rochana, Jennifer Wilcox *

Department of Energy Resources Engineering, School of Earth Sciences, Stanford University, Green Earth Sciences 065, 367 Panama Street, Stanford, CA 94305, United States

ARTICLE INFO

Article history:
Received 17 April 2010
Accepted 4 January 2011
Available online 11 January 2011

Keywords:
FeCo alloys
Density functional theory
CO adsorption energy
d-band center

ABSTRACT

FeCo catalysts are modeled for optimizing the Fischer–Tropsch synthesis process since they can be tuned to enhance CO activity and resist poisoning. The electronic properties associated with CO adsorption are studied using plane-wave density functional theory (DFT). The range of computed adsorption energies from this work falls between the CO adsorption energies on pure Fe and Co surfaces. It was found that CO prefers to adsorb on the top site of the Co surface of FeCo alloys, whereas CO has stronger adsorption on pure Fe rather than pure Co surface. The trend in adsorption energy is top-Co>hollow-Fe>top-Fe>hollow-Co>bridge-Co>bridge-Fe. This change in preferable metal for adsorption (*i.e.*, from Fe in a pure system to Co in the FeCo alloy surface in the current investigation) is due to the shift in the d-band center of the alloyed material. It implies that alloying Fe with Co changes the properties of the pure metal and ultimately affects the CO adsorption energy; however, the mechanism of adsorption remains similar and can be explained using the Nilsson–Pettersson model. Additional CO configurations consisting of hollow-site adsorption with a tilted geometry, was also investigated. The corresponding adsorption energy was found to be slightly higher than the adsorption energy when CO is adsorbed on the top-Co site.

1. Introduction

Fischer–Tropsch (FT) synthesis, a key process in transforming coal or biomass feedstocks into liquid fuels, is a catalyzed chemical reaction converting synthesis gas ($CO + H_2$), which is obtained from gasification, into various forms of liquid hydrocarbons. The current commercial FT catalysts are either cobalt (Co)-based or iron (Fe)-based catalysts. The Co-based catalysts are more active and have a longer lifetime than Fe-based. Additionally the Co-based catalysts have selectivity towards linear paraffins, while Fe-based are selective toward high-valued linear alkenes [1,2]. Due to the low H_2:CO ratio in coal-derived synthesis gas, water–gas shift (WGS) activity is a crucial step in enhancing H_2 production and leads to an increase in the H_2:CO ratio in FT synthesis. Generally, catalysts based on Fe are preferred for FT synthesis with coal-derived synthesis gas since they exhibit higher WGS reactivity. However, they are susceptible to primarily two contaminants in the synthesis gas, that is, sulfur that naturally exists in coal and biomass, and carbon which forms a carbide layer over the catalyst surface [1,2]. By considering the benefits and limitations of both catalysts, an alloy of Fe and Co is an attractive option for incorporating the individual advantages as well as suppressing their existing drawbacks.

Several experimental studies have been carried out on bimetallic FeCo alloys and the effect of relative composition on the FT reaction [3–6]. These materials have shown high activity towards FT synthesis and demonstrated promise for suppressing carbide formation thereby slowing the catalyst degradation rate [3]. However, none of these studies have provided information regarding a mechanism associated with the influences of the bimetallic properties on the specific adsorption, dissociation, and formation pathways of the FT reaction mechanism on FeCo alloys surfaces. Recently, theoretical investigations on the adsorption and dissociation of CO and H_2 on the FeCo alloy (110) surface have been conducted [7,8]. It has been shown that CO adsorption is favored at Co sites rather than Fe in the case of FeCo alloys. In contrast, other theoretical studies of CO adsorption on pure Fe(110) [9] and pure Co(0001) [10] surfaces reveal that the pure Fe surface appears to have stronger CO binding energies compared to the pure Co surface. It was concluded that the synergetic effect of the bimetallic FeCo bulk alters its physical and chemical properties compared to the pure surfaces of Fe or Co. In addition, the interaction between the neighboring Fe and Co atoms affects the local electronic structures of the different active sites on the surface and the bond strength of the adsorbed CO. Nevertheless, a fundamental understanding of the molecular-level interactions of neighboring Fe and Co atoms is still lacking and information related to CO adsorption on a variety of FeCo alloy surfaces remains scarce.

Within this work, CO adsorption on the FeCo(100) surface has been investigated and compared to the previous study of CO adsorption on the FeCo(110) surface [8]. Since true catalysts are often a combination of various surfaces due to reconfiguration upon support deposition, it is not necessarily the case that the most stable single-crystal surface is the most reactive in application. It is well

* Corresponding author. Tel.: +1 650 724 9449; fax: +1 650 725 2099.
E-mail address: jen.wilcox@stanford.edu (J. Wilcox).

0039-6028/$ – see front matter © 2011 Elsevier B.V. All rights reserved.
doi:10.1016/j.susc.2011.01.003

known that defects such as stepped, corrugated or kink sites are likely more reactive compared to their low-index counterparts [11–17]. In the current study, the less stable surface, i.e., FeCo(100) has been investigated. The analysis of the local density of states (LDOS) and charge density profile of the CO-adsorbed systems has been applied to examine the CO adsorption mechanism on the FeCo(100) surface, which is the first step in the FT synthesis process.

2. Computational methodology

All calculations are based upon plane-wave density functional theory (DFT) and performed using the Vienna *ab initio* simulation package [18–20]. The electron–ion interactions are represented by the projector-augmented wave (PAW) approach [21,22] and the exchange-correlation effects are described by the Perdew-Wang 91 (PW91) [23,24] generalized gradient approximation (GGA). The kinetic energy cutoff for the plane-wave basis set is set at 400 eV. Spin polarization is taken into account in all calculations due to the effect of the magnetic nature of the FeCo alloy. During geometry optimization, the conjugate-gradient (CG) algorithm is applied to relax the ions into their instantaneous ground state, as well as electron smearing with a width of 0.1 eV is employed via the Methfessel–Paxton technique [25] for an improved convergence. Geometry convergence is achieved when the forces on all unconstrained atoms are less than 0.01 eV/Å.

Since the typical temperature range of FT synthesis falls within 200–350 °C, the stoichiometric composition of the FeCo alloys spans from 25 to 75 at.% Fe [26]. A 50% Fe composition of FeCo, which adopts the ordered body-centered cubic (bcc)-based CsCl-B2 structure [27], has the strongest tendency to exist as an ordered alloy among the other compositions [28]. The experimental lattice constant of FeCo is 2.8504 Å [29], while previous theoretical prediction based upon DFT predicts a value of 2.8418 Å [7,8]. In this study, the calculated equilibrium lattice constant is 2.835 Å using a $11\times11\times11$ Monkhorst-Pack *k*-point mesh [30]. This value differs from the experimental and theoretical quantities by 0.54% and 0.24%, respectively.

The FeCo(100) alloy surface considered in this work was created by cleaving the bulk crystal along the (100) plane. It is important to note that the clean FeCo(100) surface is constructed from alternating layers of Co and Fe atoms and is rearranged according to a (100) pattern. As a result, there are two models of the clean FeCo(100) surface, that is, FeCo(100) with the Co atoms comprising the top layer (FeCo(100)–Co) and FeCo(100) with the Fe atoms comprising the top layer (FeCo (100)–Fe). Within the slab approximation, the 5-layer slab of FeCo (100)–Co and FeCo(100)–Fe surfaces in a 2×2 arrangement with four metal atoms per layer were used by keeping fixed the bottom two layers at their bulk position with the remaining layers relaxed. In this case, the surface energy must take into account the contribution from the unrelaxed surface. As a result, the corresponding surface energies are calculated from Eq. (1), where σ^{UR} is the surface energy of the unrelaxed surface, E_s is the total energy of the unrelaxed slab and E_B is the reference bulk energy per atom. The parameter N_{at} refers to the total number of atoms in the surface slab, the relaxation energy, E^{rel}, is the difference in the total energy of the fully relaxed slab and the unrelaxed slab, and A is the surface area [31,32].

$$\sigma = \frac{1}{A}\left(\sigma^{UR} + E^{rel}\right) \quad \text{where} \quad \sigma^{UR} = \frac{1}{2}\left(E_s - N_{at}E_B\right) \tag{1}$$

A $7\times7\times1$ *k*-point grid has been used to reduce the computational time while maintaining the accuracy of the results. It has been verified that the same lattice constant is obtained using the finer *k*-point grid, $11\times11\times11$. The calculated surface energies of the FeCo(100)–Co and FeCo(100)–Fe surfaces are 3.029 J/m^2 and 2.042 J/m^2, respectively. The additional calculation for the surface energy of FeCo(110), which has a mixture of Fe and Co atoms at the surface yields a surface energy of 2.161 J/m^2. The order of surface energies from lowest to greatest, i.e., FeCo(100)–Fe<FeCo(110)<FeCo(100)–Co, indicates that the FeCo(100)–Fe surface is most likely to exist upon cleavage of the Fe-Co alloy. This result may seem counterintuitive since the (110) surface is normally the most stable compared to other bcc surfaces; however, these surface energies are in reasonable agreement with previous spectroscopy data on the FeCo alloy. According to the surface composition of a bulk 50 Fe/50 Co by Auger electron spectroscopy [33], the surface composition was found to be 75 ± 5 at.% Fe and 25 ± 5 at.% Co suggesting that the surface is enriched with Fe. Therefore, it can be implied that the surface layer in the (100) orientation will be occupied by Fe atoms whereas the neighboring sublayer is enriched in Co atoms when the surface is exposed to a vacuum environment. It was discussed previously that the FeCo(110) is the most stable surface where the FeCo(100) surface is the next most stable [7]; however, it was not explicitly outlined which surface termination was included in the calculation of the FeCo(100) surface.

A supercell using a 4-layer slab model in a 2×2 arrangement with four metal atoms per layer was modeled for the subsequent calculation regarding the adsorption study of CO on the FeCo(100) surface. A 10-Å vacuum region was placed above the slab surface to avoid dipole interactions from periodic images. The bottom two layers were fixed at their bulk positions while the remaining top two layers in addition to the CO molecule were allowed to relax to their optimized geometries. The adsorption of CO is assumed to occur on only one side of the slab with the CO molecule adsorbed with the carbon atom of CO directed downward toward the FeCo surface. Fig. 1 shows the schematic representation of the possible adsorption sites of CO on the FeCo(100) surface with 0.25 ML and 0.50 ML coverages. Fe and Co atoms are shown by gold and blue circles, respectively. The dashed box represents the unit cell of the FeCo(100) surface viewed from the top. Each layer of a unit cell consists of four metal atoms. One CO molecule and two CO molecules adsorbed on the surface depicts 0.25 ML and 0.50 ML coverage, respectively. There are three possible adsorption locations, that is, top, bridge and hollow site. In addition, the two configurations for the 0.50 ML CO adsorption on the FeCo(100) surface are zigzag and straight configuration as shown in Fig. 1(b) and (c).

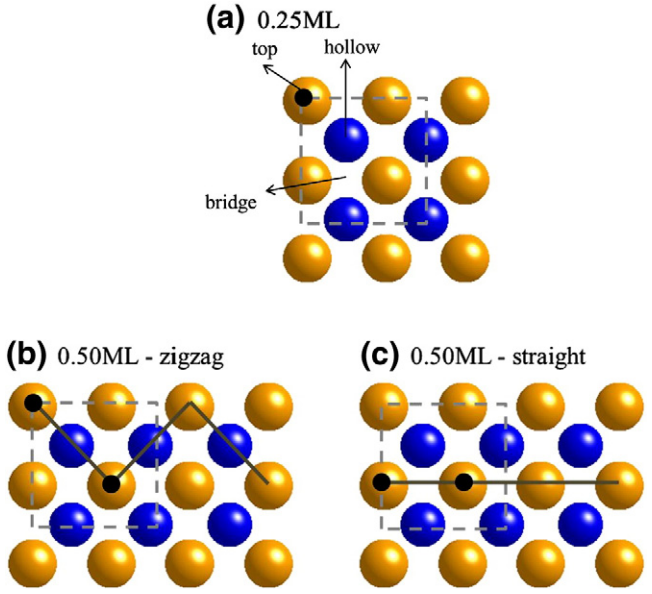

Fig. 1. Adsorption locations and configurations of CO on the FeCo(100) surface (Top view).

The associated adsorption energy is determined from Eq. (2),

$$E_{ads} = \frac{(NE(CO) + E(slab)) - E(CO + slab)}{N} \quad (2)$$

such that, *E(slab)*, *E(CO)* and *E(CO + slab)* are the total free energy of the clean surface, free CO molecules and the adsorbed CO-system, respectively. The parameter *N* is the number of CO molecules on the supercell surface. By this definition, the more positive value indicates a more preferable adsorption site. The adsorption of CO is investigated for several adsorption sites and at two surface coverages as mentioned previously.

The local density of state (LDOS) plots corresponding to the adsorption of CO molecule are examined through the optimized geometries of the CO molecule on different adsorption sites to explain the mechanism of CO adsorption on the metal slab. In addition, charge density profiles are obtained by the difference between the charge density of total system and the addition of the charge density of the bare surface and the adsorbate atoms. This information helps in visualizing the relative charge distribution during the CO adsorption process.

3. Results and discussion

3.1. Adsorption energy

The calculated adsorption energies as well as the corresponding geometry of CO on the FeCo(100) surface at various adsorption sites for the case of 0.25 ML coverage are listed in Table 1. Before discussing the CO adsorption energies on alloys, it is interesting to examine adsorption on the pure metals Fe and Co. The CO adsorption energy on the pure Fe(001) surface is 1.62 eV [34], whereas the CO adsorption energy on the pure Co(0001) surface is 1.16 eV [35]. Apparently, CO binds stronger on the pure Fe surface than the pure Co surface; however, this trend is opposite in case of the FeCo alloy as seen from Table 1, where the CO molecule prefers to bind with Co rather than with Fe on the FeCo(100) surface. This evidence confirms that alloying Fe and Co modifies the metal properties of the pure state to some extent.

To compare the trend of CO adsorption on different FeCo surfaces, adsorption energies on the FeCo(110) surfaces are also included in Table 1. Since the FeCo(110) surface naturally consists of a mixture of Fe and Co atoms in each layer, the existing adsorption sites for CO are different and only the CO adsorption energies on top-Co and top-Fe sites of the FeCo(110) surface are considered for comparison with the adsorption energies on the FeCo(100) surface. In case of the CO adsorption on the FeCo(110) surface, it was found that the top-Co site is the most energetically favorable with the Co-C bond formation preferred [8]. This is also found in the case of CO adsorption on the FeCo(100) surface where CO adsorption at the top-Co site is the most stable configuration due to its highest adsorption energy. However, this adsorption energy is found to be weaker than that of the top-Co site on the FeCo(110) surface. On the other hand, the CO adsorption energy on the top-Fe site of the FeCo(100) surface is stronger than that of the top-Fe site of the FeCo(110) surface. It is important to keep in mind that the surface of FeCo(100) is composed of the same atom type (alternating atom type per layer), whereas the FeCo(110) surface has a mixture of Fe and Co atoms. The difference in surface composition between the FeCo(100) and FeCo(110) surfaces can lead to the modification of the electronic structure of the surface atoms. The degree of modification may depend on the type of the neighboring atom, which can be different between each surface. In the case of the FeCo(110) surface, this mixture of Fe and Co atoms can alter the property of surface Co atoms such that there is an increase in local electron density in this area compared to that of the Co atoms within the FeCo(100)–Co surface, in which Co is surrounded by only Co atoms in the x and y directions. On the Pauling electronegativity scale, Co (1.880) has a slightly higher electronegativity than Fe (1.830), which is consistent with Co withdrawing electron density from nearest neighbor Fe atoms in a mixed layer, as is the case of the FeCo(110) surface. This in part explains why the adsorption energy on the top-Co site of the FeCo(110) surface is stronger than the adsorption on the top-Co site of the FeCo(100) surface. Within the CO molecule, carbon is acting as a Lewis acid and interacting strongly with the metal that exhibits the most basic character, i.e., the propensity to donate electron density. Consistent with this reasoning, the local electron density of the surface Fe atom of the FeCo(110) surface decreases compared to the surface Fe of the FeCo(100)–Fe surface. As a result, the opposite trend is observed, i.e., CO adsorbs weaker at the top-Fe site of the FeCo(110) surface than at the top-Fe site of the FeCo(100)–Fe surface. In addition, the surface properties such as the work function and d-band center will be different thereby contributing to the observed variation in CO adsorption on a particular surface.

Consider the adsorption energy of CO at higher coverage, that is, 0.50 ML as tabulated in Table 2 and recall that there are two possible CO adsorption configurations as described previously. Similar to the result of 0.25 ML CO coverage, the most preferable adsorption site is the top site with the zigzag adsorption configuration yielding the more stable configuration for CO adsorption, which is likely a result of the symmetry of the structure of the adsorbed molecule on the surface. Moreover, the CO molecule remains preferentially adsorbed on Co rather than Fe.

Table 1
Adsorption energies (eV) of CO on FeCo(100) and FeCo(110) surfaces at 0.25 ML coverage.

Adsorption site	r(C–O) (Å)	r(C–metal)[a] (Å)	h(C–metal)[b] (Å)	Adsorption energy (eV)
FeCo(100)				
top-Co	1.169	1.751	1.751	1.675
top-Fe	1.174	1.771	1.771	1.585
bridge-Co	1.186	1.914 [2]	1.431	1.510
bridge-Fe	1.191	1.943 [2]	1.492	1.455
hollow-Co	1.234	2.124 [4]	0.790	1.548
hollow-Fe	1.234	2.111 [4]	0.998	1.609
FeCo(110) [8]				
top-Co	1.168	1.766	1.766	1.721
top-Fe	1.166	1.816	1.816	1.491

[a] The bond distance between C atom and the nearest-neighbor metal atom. The number in the bracket represents the metal coordination atom.
[b] The distance between C atom and the top metal layer.

Table 2
Adsorption energies (eV) of CO on FeCo(100) surface at 0.50 ML coverage.

Adsorption site	r(C–O) (Å)	r(C–metal)[a] (Å)	h(C–metal)[b] (Å)	Adsorption energy (eV)
top-Co, zigzag	1.165	1.766	1.766	1.706
top-Co, straight	1.162	1.780	1.780	1.485
top-Fe, zigzag	1.168	1.801	1.801	1.566
top-Fe, straight	1.165	1.799	1.799	1.341
bridge-Co, zigzag	1.181	1.918 [2]	1.443	1.492
bridge-Co, straight	1.178	1.932 [2]	1.435	1.383
bridge-Fe, zigzag	1.184	1.953 [2]	1.504	1.431
bridge-Fe, straight	1.183	1.977 [2]	1.464	1.280
hollow-Co, zigzag	1.231	2.132 [4]	0.725	1.566
hollow-Co, straight	1.216	2.124 [4]	0.857	1.296
hollow-Fe, zigzag	1.244	2.135 [4]	0.735	1.449
hollow-Fe, straight	1.218	2.137 [4]	0.956	1.318

[a] The bond distance between C atom and the nearest-neighbor metal atom. The number in the bracket represents the metal coordination atom.
[b] The distance between C atom and the top metal layer.

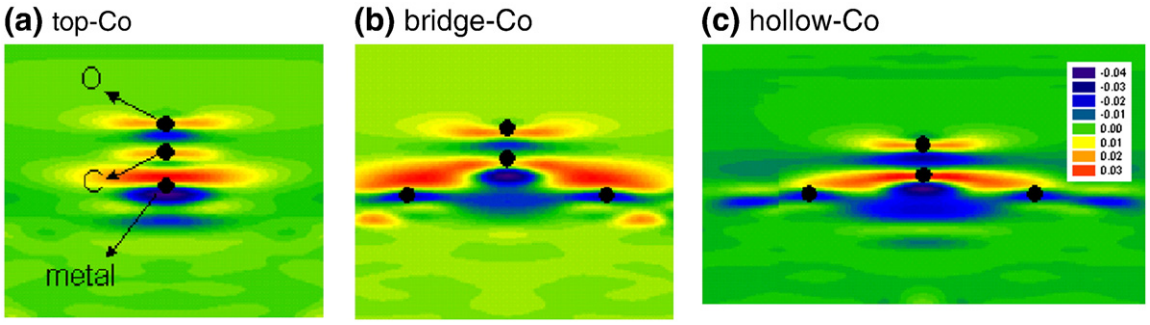

Fig. 2. Charge density profiles for CO-adsorbed systems at 0.25 ML coverage. The definition of color spectrum is as follows: the minus sign represents charge loss and the plus sign represents charge gain.

3.2. Electronic structure and mechanism of CO adsorption on the FeCo(100) alloy

Charge density profiles for the CO-adsorbed systems for top-, bridge- and hollow-Co sites with 0.25 ML coverage are shown in Fig. 2. The bond-breaking between the C and O atoms is clearly seen as well as the bond formation between the C atom and associated metal atoms. In addition, the charge accumulation of the O atom is observed and corresponds to a lone electron pair from the breaking of the internal C–O bond.

Further explanation concerning the adsorption mechanism as well as the site preference for CO adsorption on the FeCo alloy surface can be extracted from the local density of states (LDOS) plots corresponding to CO adsorbed at various adsorption locations. Fig. 3(a) shows the LDOS plots of the CO free-gas molecule, where each individual peak represents the interacting molecular orbitals of the CO molecule. These orbitals are termed 4σ, 1π, 5σ and 2π and are located at approximately −5, −3, 0 and 7 eV, respectively. The 5σ orbital is known as the highest occupied molecular orbital (HOMO) of the CO free-gas molecule since it resides exactly at the fermi level (0 eV), while the 2π orbital is the lowest unoccupied molecular orbital (LUMO). Fig. 3(b) and (c) illustrate the LDOS plots of the clean FeCo (100)–Co and FeCo(100)–Fe surfaces, respectively. Fig. 4 illustrates the LDOS plots of CO-adsorbed surfaces of the FeCo(100) surface at top sites with 0.25 ML coverage. The interactions between the adsorbed CO molecule and each surface occur at two distinct locations with electronic energies of approximately −9 eV (4σ) and −6 eV (5σ and 1π). At the 5σ peak, a significant change regarding the degree of polarization of the CO molecule can be noticed. In spite of having the 5σ orbital polarizing towards the C atom as it is prior to adsorption, it instead polarizes towards the O atom after adsorption. The intensity weakening associated with the π-band tailing off to the Fermi level is also observed in all cases. The additional state at −4 eV with low intensity is found in the σ-system after adsorption. This state represents the antibonding orbital between the CO molecule and metal. Considering the adsorption on the FeCo(100)–Co surface, the Co atoms appear to play a more important role than the Fe atoms as can be seen from the relative peak intensity of Fe and Co *d* orbitals. This observation is opposite when CO adsorbs on the top-Fe site in which the peak intensity of Fe *d* orbital is higher.

The CO adsorption on transition metals is commonly described by the traditional Blyholder model [36] where two valence states, that is, the filled 5σ and the empty $2\pi^*$ states play an important role in coupling to the metal *d*-states. Charge donation from the 5σ orbital to the metal *d*-states is balanced by a back-donation into the molecular $2\pi^*$ which results in a weakening of the internal CO molecular bond. However, it has been found that the coupling of the $2\pi^*$ orbital to the metal *d*-bands is much stronger than the coupling of the 5σ orbital for CO adsorption on the late transition metals [37]. The Blyholder model has been recently modified by describing the role of the σ- and π-contribution and named as the Nilsson–Pettersson model [38]. The σ-donation and the π-interaction are responsible for the repulsion and the attraction, respectively. The electronic configuration of the CO-adsorbed system is arranged towards minimizing the σ-repulsion,

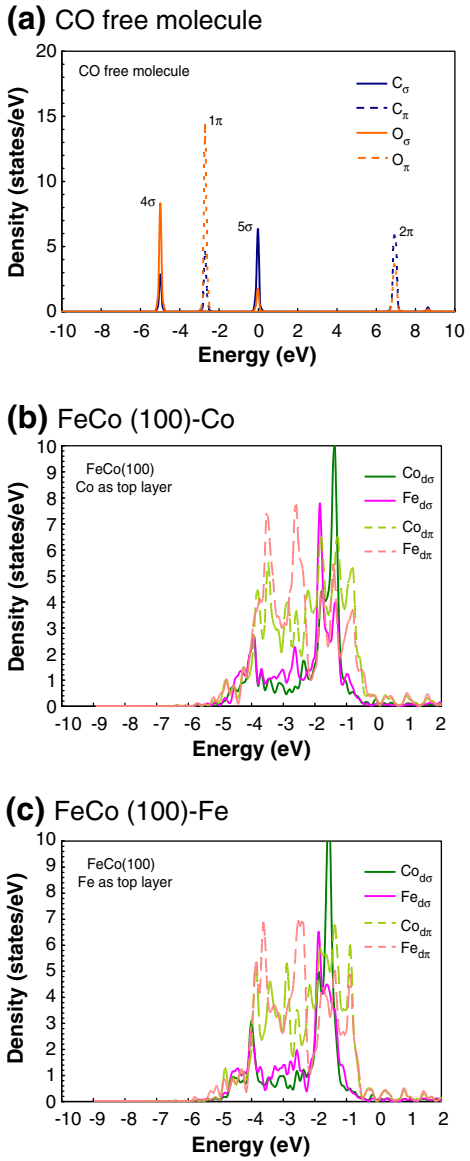

Fig. 3. LDOS plots of σ- and π-systems of CO free molecule, clean FeCo(100)–Co and FeCo(100)–Fe surfaces.

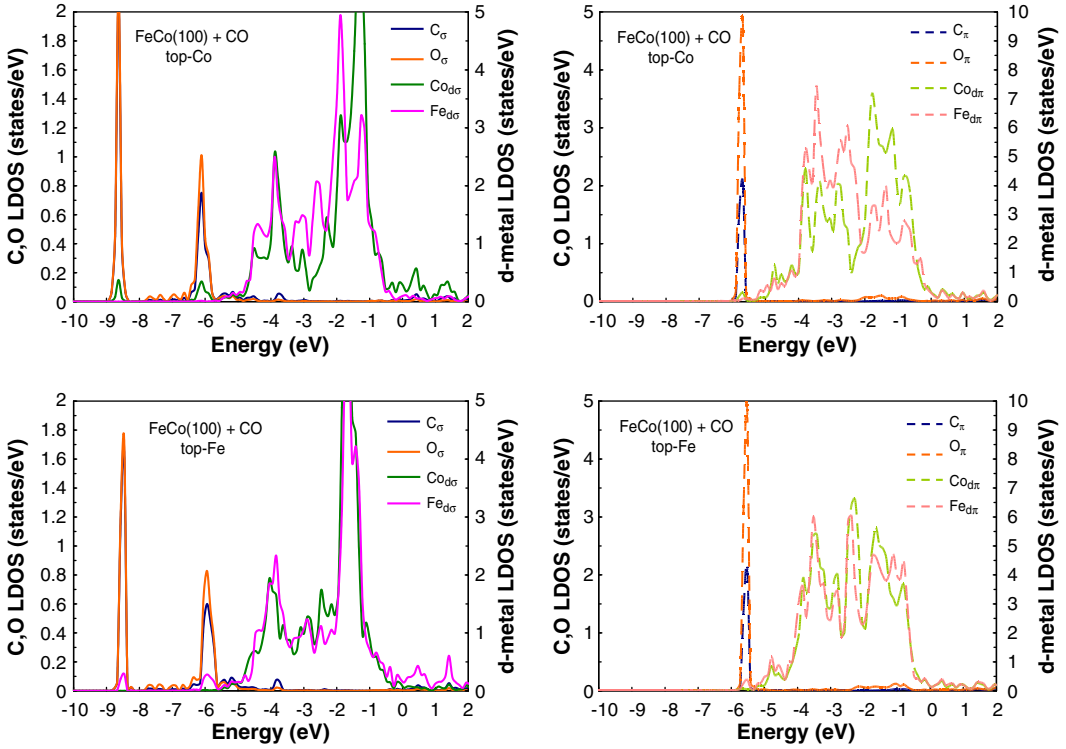

Fig. 4. LDOS plots of σ- and π-systems of CO-adsorbed system of the FeCo(100)–Co and FeCo(100)–Fe surfaces after CO adsorption at 0.25 ML on top sites.

while maximizing the π-bonding. The π-system takes into account the rehybridization of the 1π and $2\pi^*$ orbitals which breaks the internal π-bond. One part of the electron pair becomes a lone-pair orbital on the O atom and the other part creates a radical state for the C atom, which is free for bonding as can be seen from Fig. 2. As seen in Fig. 4, the weak intensity of the π-band at about −2 eV, which is tailing off to the Fermi level, represents a lone-pair orbital on the O atom. The LDOS plots for the 0.25 ML CO-adsorbed system at the bridge and hollow sites are attached as supplementary illustrations. The same observation as that of CO adsorption on top sites can be drawn as the tailing π-band is clearly apparent. In addition, the metal *d*-states at approximately −9 eV and −10 eV are found in the case of CO adsorption at the higher coordination sites. This small extra peak is overlapping with the 4σ-state of the adsorbed CO molecule, which refers to the interaction between the CO molecule and the neighboring metal atoms. However, it appears that the $2\pi^*$ orbital becomes more involved in the π-interaction when CO adsorbs on the higher coordination site such as the hollow site. Generally, the degree of π-interaction increases with increasing metal coordination [38,39]. It has been known that DFT may not provide an accurate description of the HOMO–LUMO gap for the CO gas-phase molecule [40]. An overestimation of the interaction between the $2\pi^*$ orbital and the metal d-electrons for the high coordination site may be a result of the underestimation of the HOMO–LUMO gap for CO where the underestimated HOMO position is predicted [35]. As a result, an inconsistency of the C-metal bond formation preference at the hollow site occurs when the hollow-Fe site is more favorable than the hollow-Co site at 0.25 ML coverage; meanwhile, the opposite observation is found at 0.50 ML coverage. This issue may be resolved by applying a molecular DFT + U approach so that the HOMO–LUMO gap for CO and the strength of chemisorption can be corrected for high coordination metal sites [40] or by performing the random phase approximation (RPA) calculation where the right decay behavior outside the metal surface can be achieved by combining the exact exchange from the Hartree–Fock (HF) expression with the correlation energy based on the renormalized Coulomb potential [41]. This method can be used as the post-correction to the preceding standard DFT calculation since it has been shown to improve the adsorption energy and the site preference of CO on metallic surfaces [42].

Consider the electronic structure of the CO adsorption at higher coverages. The LDOS plots of 0.50 ML CO coverage for the possible configurations can be found in the supplementary illustrations. It is obvious that the characteristics of these LDOS plots are more complicated than the cases for the 0.25 ML CO coverage. However, the basic observation, that is, the polarization towards the O atom of the 5σ orbital and the π-band tailing towards the Fermi level is observed.

3.3. Effect of alloying on pure metal properties

Alloying Fe and Co does not change the mechanism of CO adsorption on their corresponding pure metal surfaces; however, the electronic properties of the alloy can be altered from the original properties of the pure metal surface and affect the adsorption energy as discussed previously. When CO adsorbs on the alloy of Fe and Co, it prefers to bind to the Co-site. Meanwhile, the opposite trend is exhibited if CO adsorbs on a pure Fe and Co surface. In this section, two important properties – work function (Φ) and the d-band center of metal (ε_d) – are discussed in detail. The shift in the work function affects the reactivity of a transition metal surface, more specifically, the bonding between the CO molecule and the metal surface can be strengthened or weakened by changing the location of the d-band center of the metal.

3.3.1. Work function (Φ)

The work function is defined as the minimum energy that is required to remove an electron from the highest occupied energy level in the solid to the vacuum. It can be calculated from the difference between the potential in the vacuum region and the Fermi level. The work function of the pure Co(0001) and Fe(001) surfaces as well as the calculated work function of the FeCo(001) surface are listed in Table 3. Notice that the work function of the alloy is lower than the value of the pure materials. It can be inferred from this difference that less energy is required to remove an electron from the

Table 3
Work function (eV) of materials.

Materials	Work function, Φ (eV)
Co(0001)	5.0 (exp) [56,57]
	5.05–5.52 (theory) [58–60]
Fe(001)	4.67 (exp) [56]
	4.5 (exp) [57]
	4.29–4.70 (theory) [58,60–62]
FeCo(100)–Co	4.25
FeCo(100)–Fe	4.19

Table 4
d-band center (ε_d) of materials.

Materials	ε_d (eV)	Adsorption energy (eV) on top location at 0.25 ML
FeCo(100)–Co	−1.74	1.67
FeCo(100)–Fe	−2.26	1.58
Fe(001)	−0.92*	1.62†
Co(0001)	−1.17**	1.16††

* Ref. [65], ** Ref. [66].
† Ref. [34], †† Ref. [35].

alloy surface implying that the surface sites may be more likely to exhibit a basic nature, which is preferred for a strong interaction with the acidic carbon atom of CO. It is well-known that the difference in the range of energy in the band structure and the Fermi level is responsible for the difference in work function for different metals [43]. Therefore, it can be expected that the energy in the band structure as well as the Fermi level of the FeCo(100) surface are modified after alloying Fe and Co.

The CO molecule is considered to be an electronegative adsorbate when it interacts with the carbon atom directed downward towards metal surface. The molecule withdraws the electron density from the metal implying that a material with a lower work function is more favorable for CO adsorption since the electrons can be pulled from the surface more easily. Those electrons interact with the corresponding σ and π orbitals of the CO molecule. According to Table 3, the FeCo(100) surface is more reactive for CO adsorption than either the Co(0001) or Fe(001) surface due in part to its lower work function. Moreover, the FeCo(100)–Fe surface tends to be more reactive for CO adsorption than the FeCo(100)–Co surface. Since this work is purely based on thermodynamic equilibrium, that is, the stable adsorption configuration of CO, more studies related to the dissociation and subsequent C–C coupling or C–H bonding pathways are required to determine the turnover frequency of the catalyst. The surface needs to bind strong enough for stretching the C–O bond, but not too strong that it inhibits further C reactivity for the crucial next steps of the FT process.

Also, the work function is not the only property that determines the effect of alloying towards the mechanism of CO adsorption. Since the FeCo(100) surface is more reactive than the pure metal surface, the CO adsorption energies of the FeCo(100) surface fall between the range of CO adsorption energies of the pure Fe(001) and Co(0001) surfaces. It is also found that CO binds stronger on the FeCo(100)–Co surface even though it tends to be less reactive according to the lower work function. The next section discusses the d-band center, which is another property of the metal that is related to the adsorption energy and corresponding mechanism of the CO-adsorbed system.

3.3.2. The metal's d-band center (ε_d)

Nørskov and co-workers previously showed that the adsorption energy consists of two elements, that is, the coupling to the *s* states of the transition metal and the extra coupling to the *d* states [44–50]. However, the first contribution from the *s* state is relatively similar for each transition metal. Consequently, only the coupling to the *d* electrons of the transition metals is taken into account for considering the trend in adsorption energy and the reactivity of the surfaces [44,49,50]. The location of the d-band center (ε_d) relative to the Fermi level can be used to describe the bonding strength between the adsorbate and the metal surface. As the d-band center moves closer to the Fermi level, the bond between the adsorbate and the metal surface becomes stronger since the antibonding states exist above the Fermi level and these states are empty. The opposite trend is observed when the d-band center is shifted down (further from the Fermi level) and the antibonding states become filled so that the bond between the metal surface and the adsorbate is weaker [44].

The d-band center is the centroid of the d-orbital density of states and it is calculated by taking the first moment of the projected density of states up to the Fermi level [51]. Table 4 lists the d-band center for the surface metal atom and the example of CO adsorption at the top site of each surface is considered. The location of the d-band center of the FeCo(100)–Co surface is closer to the Fermi level when compared to the d-band center of the FeCo(100)–Fe surface; hence, a stronger CO adsorption energy on the FeCo(100)–Co surface is observed. Comparing the location of the d-band center of the surface of FeCo(100)–Fe versus the d-band center of the pure Fe(001) surface, according to Table 4, it is found that the d-band center of the FeCo(100)–Fe surface is located further away from the Fermi level than the d-band center of the pure Fe(001) surface. Therefore, the weaker adsorption energy is obtained in case of CO adsorption on the FeCo(100)–Fe surface. This observation indicates that the effect of alloying towards the change in electronic structure of the alloy surface from the pure metal surface and its ultimate consequence on the adsorption energy of CO.

3.4. Other CO adsorption configurations on the FeCo(100) surface

It has been known that CO typically binds in the upright position with the C-end down toward the top site of several transition metals surfaces [35]. Typically, the CO adsorption energy is rather similar at top and bridge sites and slightly less stable at hollow sites [38]. Interestingly, recent theoretical studies [52–54] reveal the unique CO geometry after adsorption on the (100) surfaces of body-centered cubic transition metals and alloys. It has been shown that the adsorption of CO on the bcc(100) metal surface differs from that of fcc metals and even bcc(110) surfaces. The most stable site for molecular CO adsorption is the fourfold hollow site with tilting angles with respect to the surface normal in the range of 47°–58° depending on the type of metal. The carbon atom is in the fourfold hollow site, whereas the oxygen atom is at the bridge position. Only at monolayer coverage does co-adsorption in a perpendicular mode occur [55]. In addition, the tilted geometry is observed only when CO binds to the high coordination adsorption sites, i.e., bridge and hollow sites, with oxygen taking part directly in the bonding mechanism with the metal. Additional calculations where the CO molecule was placed at the hollow site with an initial tilting angle of approximately 45° from the surface normal were performed at 0.25 ML coverage and the results are shown in Table 5. It is important to note that CO adsorption at the hollow-Fe site with tilted geometry is more stable than adsorption

Table 5
Adsorption energies (eV) of CO on FeCo(100) at hollow site with tilting geometry.

Adsorption site	r(C–O) (Å)	r(C–metal)[a] (Å)	h(C–metal)[b] (Å)	θ[c] (°)	Adsorption energy (eV)
hollow-Co/tilt	1.272	1.956 [2] 2.232 [2]	0.716	46.9	1.62
hollow-Fe/tilt	1.307	1.963 [2] 2.200 [1] 2.243 [1]	0.707	52.9	1.71

[a] The bond distance between C atom and the nearest-neighbor metal atom. The number in the bracket represents the metal coordination atom.
[b] The distance between C atom and the top metal layer.
[c] θ is the angle between the surface normal and the CO molecular axis.

at the hollow-Co site with a tilting angle and even stronger than the adsorption on the top-Co site. Considering the C–O bond distance after adsorption, the CO molecule is activated in all possible adsorption modes as noticed from an increase in the CO bond distance compared to its bond distance in the gas phase.

4. Conclusions

The adsorption mechanism and electronic structure of CO adsorption on FeCo(100) alloys have been investigated using spin-polarized DFT calculations. It has been found that the FeCo(100)–Fe surface is more stable than the FeCo(100)–Co surface. However, it is important to keep in mind that these surface energies were calculated at the zero-temperature and zero-pressure environment. To take into account the realistic environment for Fischer–Tropsch synthesis, one can include the *ab initio* thermodynamic concept for the surface energy calculation [63] where the stability of the surface as well as the surface composition can be determined at the finite temperature and pressure. The appropriate thermodynamic potential to consider is the Gibbs free energy. The Gibbs free energy of the entire system can be divided into contributions from the bulk solid phase, the gas phase and the surface. The Gibbs free energy for the gas species that is in direct contact with the surface of study is equivalent to the chemical potential of each species (i.e., CO, H_2 and hydrocarbon gases for the Fischer–Tropsch environment). As a result, the surface energy with respect to an equilibrium with the environment can be determined by Eq. (3),

$$\gamma = \frac{1}{A}\left[G_{syst}(T,p,N_M,N_i) - N_M\mu_M(T,p) - \sum_i N_i\mu_i(T,p)\right]. \quad (3)$$

According to the adsorption energy of the corresponding systems, CO preferentially adsorbs on the Co-site rather than the Fe-site. This finding is opposite that of CO adsorption on the pure surface, in which Fe exhibits a stronger adsorption energy. The top sites appear to be the most stable for CO adsorption at both 0.25 ML and 0.50 ML coverages. All of these adsorption configurations appear to be CO activation sites; however, when the CO molecule was placed at the hollow site at a tilting angle, the adsorption energy was found to be strongest. Analysis of the LDOS of the surface atoms and the charge density profiles shows that the bond-breaking of the CO molecule results in a lone-electron orbital at the O atom and the radical-state C atom. The latter can form a bond with the metals on the surface. This finding is qualitatively in reasonable agreement with the Nilsson–Pettersson model. Alloying Fe and Co together does not affect the mechanism of CO adsorption on the surface; nevertheless, the electronic properties of the alloy are different from the pure metal surface. The work function of the FeCo(100) alloy is smaller than the value of the pure Fe or Co surface. It could be implied that the FeCo (100) surface becomes more reactive. Another important electronic property that defines the surface adsorption preference is the d-band center of the surface metal. It was found that the d-band center of the FeCo(100)–Fe surface is closer to the Fermi level compared to the d-band center of the pure Fe(001) surface and the stronger adsorption of CO on the FeCo(100)–Fe surface is evident. It is important to note that alloying Fe and Co together can significantly change the adsorption strength of CO as observed from the switch of the preferable adsorption surface. In future work, DFT + U as well as the inclusion of the RPA calculations as the post-correction to the preceding DFT calculation will be investigated for the correction of the adsorption energy especially in case of adsorption at the hollow site.

It is worth keeping in mind that this study focused strictly on the CO adsorption mechanism, which is the very first step of the CO activation during the FT process. The CO molecule should not bind too strong to the surface so that it cannot dissociate and form new bonds with carbon or hydrogen. This work represents an example of how the properties of a metal might be tuned for optimal CO-surface reactivity via alloying. So far, the FeCo alloys have been studied without support or promoter effects. In reality, catalyst surfaces can restructure upon deposition onto a support, which likely influences the reactivity of particular reaction. For example, the addition of aluminum oxide with certain pretreatment conditions, in which Al_xO_y-supported Fe(110) was exposed to an oxidizing environment, can restructure the initially inactive Al_xO_y/Fe(110) catalyst and enhance the ammonia synthesis reactivity by approximately a 400-fold increase compared with clean the Fe(110) surface [64]. Future work will involve the investigation of support/promoter effects on catalyst reactivity.

Acknowledgements

The authors would like to acknowledge the financial support of Chevron Corporation in the form of a graduate fellowship and the computer resources provided by the Stanford Center for Computational Earth & Environment Science (CEES) in the School of Earth Sciences at Stanford University. We also would like to thank Dr. Shela Aboud for her insight and helpful discussions.

Appendix A. Supplementary data

Supplementary data to this article can be found online at doi:10.1016/j.susc.2011.01.003.

References

[1] S. Li, S. Krishnamoorthy, A. Li, G.D. Meitzner, E. Iglesia, J. Catal. 206 (2002) 202.
[2] M.E. Dry, Fischer–Tropsch Technology, in: A.P. Steynberg, M.E. Dry (Eds.), Elsevier, Amsterdam, 2005, p. 533, Vol. 152.
[3] J.A. Amelse, L.H. Schwartz, J.B. Butt, J. Catal. 72 (1981) 95.
[4] K.B. Arcuri, L.H. Schwartz, R.D. Piotrowski, J.B. Butt, J. Catal. 85 (1984) 349.
[5] T.A. Lin, L.H. Schwartz, J.B. Butt, J. Catal. 97 (1986) 177.
[6] J.B. Butt, T.A. Lin, L.H. Schwartz, J. Catal. 97 (1986) 261.
[7] J.M.H. Lo, T. Ziegler, J. Phys. Chem. C 112 (2008) 3667.
[8] J.M.H. Lo, T. Ziegler, J. Phys. Chem. C 112 (2008) 3679.
[9] A. Stibor, G. Kresse, A. Eichler, J. Hafner, Surf. Sci. 507–510 (2002) 99.
[10] Q. Ge, M. Neurock, J. Phys. Chem. B 110 (2006) 15368.
[11] F. Besenbacher, I. Chorkendorff, B.S. Clausen, B. Hammer, A. Molenbroek, J.K. Nørskov, I. Stensgaard, Science 279 (1998) 1913.
[12] S. Dahl, A. Logadottir, R.C. Egeberg, J.H. Larsen, I. Chorkendorff, E. Törnqvist, J.K. Nørskov, Phys. Rev. Lett. 83 (1999) 1814.
[13] B. Hammer, Phys. Rev. Lett. 83 (1999) 3681.
[14] H.S. Taylor, Proc. R. Soc. London Ser. A 108 (1925) 105.
[15] A.T. Gwathmey, R.E. Cunningham, Adv. Catal. 10 (1958) 57.
[16] J.T. Yates Jr., J. Vac. Sci. Technol. A 13 (1995) 1359.
[17] T. Zambelli, J. Wintterlinn, J. Trost, G. Ertl, Science 273 (1996) 1688.
[18] G. Kresse, J. Hafner, Phys. Rev. B 48 (1993) 13114.
[19] G. Kresse, J. Furthmüller, Comput. Mater. Sci. 6 (1996) 15.
[20] G. Kresse, J. Furthmüller, Phys. Rev. B 54 (1996) 11169.
[21] P.E. Blöchl, Phys. Rev. B 50 (1994) 17953.
[22] G. Kresse, D. Joulbert, Phys. Rev. B 59 (1999) 1758.
[23] J.P. Perdew, J.A. Chevary, S.H. Vosko, K.A. Jackson, M.R. Pederson, D.J. Singh, C. Fiolhais, Phys. Rev. B 46 (1992) 6671.
[24] Y. Wang, J.P. Perdew, Phys. Rev. B 44 (1991) 13298.
[25] M. Methfessel, A.T. Paxton, Phys. Rev. B 40 (1989) 3616.
[26] I. Ohnuma, H. Enokia, O. Ikeda, R. Kainuma, H. Ohtani, B. Sundaman, K. Ishida, Acta Mater. 50 (2002) 379.
[27] T. Massalski, Binary Alloy Phase Diagrams, ASM International, Ohio, 1990, 2nd edition.
[28] A. Díaz-Ortiz, R. Drautz, M. Fähnle, H. Dosch, J.M. Sanchez, Phys. Rev. B 73 (2006) 224208.
[29] P. Villars, L.D. Calvert, Pearson's Handbook of Crystallographic Data for Intermetallic Phases, ASM International, Ohio, 1991, 2nd edition.
[30] H.J. Monkhorst, J.D. Pack, Phys. Rev. B 13 (1976) 5188.
[31] G. Santarossa, A. Vargas, M. Iannuzzi, C.A. Pignedoli, D. Passerone, A. Baiker, J. Chem. Phys. 129 (2008) 234703.
[32] A. Eichler, VASP Hands on Session III, Institut für Materialphysik and Center for Computational Materials Science, Universität Wien, Austria, 2003, page 6.
[33] J.K. Morán-López, H. Wise, Appl. Surf. Sci. 4 (1980) 93.
[34] S.K. Nayak, M. Nooijen, S.L. Bernasek, P. Blaha, J. Phys. Chem. B 105 (2001) 164.
[35] F. Abild-Pedersen, M.P. Andersson, Surf. Sci. 601 (2007) 1747.
[36] G. Blyholder, J. Phys. Chem. 68 (1964) 2772.
[37] B. Hammer, Y. Morikawa, J.K. Nørskov, Phys. Rev. Lett. 76 (1996) 2141.
[38] A. Nilsson, L.G.M. Pettersson, Chemical Bonding at Surfaces and Interfaces, in: A. Nilsson, L.G.M. Pettersson, J.K. Nørskov (Eds.), 1st edition, Elsevier, Amsterdam, 2008, p. 57.
[39] S.E. Mason, I. Grinberg, A.M. Rappe, Phys. Rev. B 69 (2004) 161401(R).

[40] M. Gajdoš, J. Hafner, Surf. Sci. 590 (2005) 117.
[41] M. Rohlfing, T. Bredow, Phys. Rev. Lett. 101 (2008) 266106.
[42] X. Ren, P. Rinke, M. Scheffler, Phys. Rev. B 80 (2009) 045402.
[43] E.M. McCash, Surface Chemistry, 1st edition, 2001, Oxford University Press, Great Britain.
[44] B. Hammer, J.K. Nørskov, Adv. Catal. 45 (2000) 71.
[45] B.I. Lundqvist, O. Gunnarsson, H. Hjelmberg, J.K. Nørskov, Surf. Sci. 89 (1979) 196.
[46] B. Hammer, J.K. Nørskov, Chemisorption and Reactivity on Supported Clusters and Thin Films, in: R.M. Lambert, G. Pacchioni (Eds.), Kluwer Academic, Dordrecht, 1997, p. 285.
[47] J.K. Nørskov, Rep. Prog. Phys. 53 (1990) 1253.
[48] S. Holloway, B.I. Lundqvist, J.K. Nørskov, *Proceedings of the International Congress on Catalysis*, Verlag Chemie Weinhem Berlin, 1984, p. 85, Vol. 4.
[49] B. Hammer, J.K. Nørskov, Surf. Sci. 343 (1995) 211.
[50] B. Hammer, J.K. Nørskov, Surf. Sci. 359 (1995) 306.
[51] B. Hammer, O.H. Nielsen, J.K. Nørskov, Catal. Lett. 46 (1997) 31.
[52] F.J.E. Scheijen, D. Curulla Ferré, J.W. Niemantsverdriet, J. Phys. Chem. C 113 (2009) 11041.
[53] F.J.E. Scheijen, J.W. Niemantsverdriet, D. Curulla Ferré, J. Phys. Chem. C 112 (2008) 7436.
[54] F.J.E. Scheijen, J.W. Niemantsverdriet, D. Curulla Ferré, J. Phys. Chem. C 111 (2007) 13473.
[55] T.C. Bromfield, D. Curulla Ferré, J.W. Niemantsverdriet, Chemphyschem 6 (2005) 254.
[56] Online CRC Handbook of Chemistry and Physics, 90th edition, 2009–2010.
[57] H.B. Michaelson, J. Appl. Phys. 48 (1977) 4729.
[58] M. Aldén, S. Mirby, H.L. Skriver, N.M. Rosengaard, B. Johansson, Phys. Rev. B 46 (1992) 6303.
[59] C. Li, A.J. Freeman, C.L. Fu, J. Magn. Mat 75 (1988) 53.
[60] R. P. Dooley, Ph.D. Dissertation in *Surface Magnetism of Ni(001), Co(001), and Fe(001): An Embedding Green Function Approach* (2007), Department of Physics, Baylor University, Texas, USA.
[61] S. Ohnishi, A.J. Freeman, M. Weinert, Phys. Rev. B 28 (1983) 3356.
[62] O. Eriksson, A.M. Boring, R.C. Albes, G.W. Fernando, B.R. Cooper, Phys. Rev. B 46 (1992) 6303.
[63] J. Rogal, K. Reuter, Ab Initio Atomistic Thermodynamics for Surfaces: A Primer, Educational Notes RTO-EN-AVE-142, Paper 2, Neuilly-sur-Seine, France, 2007.
[64] D.R. Strongin, J. Carrazza, S.R. Bare, G.A. Somorjai, J. Catal. 103 (1987) 213.
[65] H.Y. Ma, G.C. Wang, Y. Morikawa, J. Nakamura, Sci. China. Ser. B Chem 52 (2009) 1427.
[66] A. Ruban, B. Hammer, P. Stoltze, H.L. Skriver, J.K. Nørskov, J. Mol. Catal. A Chem. 115 (1997) 421.